

Marburg Virus Glycoprotein GP2: pH-Dependent Stability of the Ectodomain α -Helical Bundle

Joseph S Harrison, Jayne F. Koellhoffer, Kartik Chandran, and Jonathan R. Lai

Biochemistry, **Just Accepted Manuscript** • DOI: 10.1021/bi3000353 • Publication Date (Web): 27 Feb 2012

Downloaded from <http://pubs.acs.org> on March 6, 2012

Just Accepted

“Just Accepted” manuscripts have been peer-reviewed and accepted for publication. They are posted online prior to technical editing, formatting for publication and author proofing. The American Chemical Society provides “Just Accepted” as a free service to the research community to expedite the dissemination of scientific material as soon as possible after acceptance. “Just Accepted” manuscripts appear in full in PDF format accompanied by an HTML abstract. “Just Accepted” manuscripts have been fully peer reviewed, but should not be considered the official version of record. They are accessible to all readers and citable by the Digital Object Identifier (DOI®). “Just Accepted” is an optional service offered to authors. Therefore, the “Just Accepted” Web site may not include all articles that will be published in the journal. After a manuscript is technically edited and formatted, it will be removed from the “Just Accepted” Web site and published as an ASAP article. Note that technical editing may introduce minor changes to the manuscript text and/or graphics which could affect content, and all legal disclaimers and ethical guidelines that apply to the journal pertain. ACS cannot be held responsible for errors or consequences arising from the use of information contained in these “Just Accepted” manuscripts.

1
2
3
4
5
6
7
8
9
10
11 Marburg Virus Glycoprotein GP2: pH-Dependent
12
13
14
15 Stability of the Ectodomain α -Helical Bundle[†]
16
17
18
19

20
21 *Joseph S. Harrison,[‡] Jayne F. Koellhoffer,[‡] Kartik Chandran,[§] and Jonathan R. Lai^{‡,*}*
22

23
24 [‡]Department of Biochemistry, and [§]Department of Microbiology and Immunology, Albert Einstein
25

26
27 College of Medicine, 1300 Morris Park Avenue, Bronx, NY 10461
28

29
30 *To whom correspondence should be addressed: Email: jon.lai@einstein.yu.edu. Phone: 718-430-8641.
31

32 Fax: 718-430-8565.
33

34
35
36 † This work was funded by the Albert Einstein College of Medicine, and the National Institutes of
37 Health (R01-AI088027 to K. C. and R01-AI090249 to J. R. L.). J. S. H. was supported in part by NIH
38 Molecular Biophysics Training Grant T32-GM008572, and J. F. K. by NIH Medical Scientist Training
39 Grant T32-GM007288.
40
41
42
43
44

45
46 **RECEIVED DATE (to be automatically inserted after your manuscript is accepted if required**
47 **according to the journal that you are submitting your paper to)**
48

49
50
51
52 Running Title: Stability Studies on the Marburg Virus GP2 Ectodomain.
53

54
55 Note: The authors declare no competing financial interest.
56
57
58
59
60

ABBREVIATIONS

1
2
3 MARV, Marburg virus; EBOV, Ebola virus; CatL, Cathepsin L; CatB, Cathepsin B; NPC-1, Neimann-
4
5 Pick C1; NHR, N-heptad repeat; CHR, C-heptad repeat; SFV, Semliki Forest Virus; IPTG, isopropyl- β -
6
7 D-thiogalactopyranoside; GdnHCl, guanidine HCl; CD, circular dichroism; AU, analytical
8
9 ultracentrifugation; ASLV, avian sarcoma leukosis virus; THP, tris(hydroxypropyl)phosphine;
10
11 MoMLV, murine moloney leukemia virus.
12
13
14
15
16
17
18
19
20
21
22
23
24
25
26
27
28
29
30
31
32
33
34
35
36
37
38
39
40
41
42
43
44
45
46
47
48
49
50
51
52
53
54
55
56
57
58
59
60

ABSTRACT

1
2
3 Marburg virus (MARV) and Ebola virus (EBOV) constitute the family *Filoviridae* of enveloped
4
5 viruses (filoviruses) that cause severe hemorrhagic fever. Infection by MARV is required for fusion
6
7 between the host cell and viral membranes, a process that is mediated by the two subunits of the
8
9 envelope glycoprotein GP1 (surface subunit) and GP2 (transmembrane subunit). Upon viral attachment
10
11 and uptake, it is believed that the MARV viral fusion machinery is triggered by host factors and
12
13 environmental conditions found in the endosome. Next, conformational rearrangements in the GP2
14
15 ectodomain result in the formation of a highly stable six-helix bundle; this refolding event provides the
16
17 energetic driving force for membrane fusion. Both GP1 and GP2 from EBOV have been extensively
18
19 studied, but there is little information available for the MARV glycoproteins. Here we have expressed
20
21 two variants of the MARV GP2 ectodomain in *Escherichia coli* and analyzed their biophysical
22
23 properties. Circular dichroism indicates that the MARV GP2 ectodomain adopts an α -helical
24
25 conformation, and one variant sediments as a trimer by equilibrium analytical ultracentrifugation.
26
27 Denaturation studies indicate the α -helical structure is highly stable at pH 5.3 (unfolding energy, ΔG_{unf} ,
28
29 H_2O , of 33.4 ± 2.5 kcal/mol and melting temperature, T_m , of 75.3 ± 2.1 °C for one variant). Furthermore,
30
31 we found the α -helical stability to be strongly dependent on pH with higher stability under lower pH
32
33 conditions (T_m values ranging from ~92 °C at pH 4.0 to ~38 °C at pH 8.0). Mutational analysis suggests
34
35 two glutamic acid residues (E579 and E580) are partially responsible for this pH-dependent behavior.
36
37 Based on these results, we hypothesize that pH-dependent folding stability of the MARV GP2
38
39 ectodomain provides a mechanism to control conformational preferences such that the six-helix bundle
40
41 ‘post-fusion’ state is preferred under conditions of appropriately matured endosomes.
42
43
44
45
46
47
48
49
50
51
52
53
54
55
56
57
58
59
60

1
2
3
4
5
6
7
8
9
10
11
12
13
14
15
16
17
18
19
20
21
22
23
24
25
26
27
28
29
30
31
32
33
34
35
36
37
38
39
40
41
42
43
44
45
46
47
48
49
50
51
52
53
54
55
56
57
58
59
60

Marburg virus (MARV) and the related Ebola virus (EBOV) belong to the family *Filoviridae* of enveloped viruses that cause a rapidly progressing hemorrhagic fever with human case fatalities of 50-90% (1, 2). Similar to other enveloped viruses, infection by MARV requires coordinated conformational changes in the envelope glycoproteins that ultimately result in fusion between the viral and cellular membranes (3 – 6). The envelope glycoprotein spike of MARV and EBOV consists of three copies each of a surface subunit (GP1) and a transmembrane subunit (GP2) that anchors the spike to the viral membrane (3, 5, 7 – 11). Structural and biochemical work EBOV GP1/GP2 has demonstrated that, prior to membrane fusion, the viral particle must first be internalized into cellular endosomes or lysosomes where host cysteine proteases cathepsins L and B (CatL and CatB) remove all but a small (~17 kDa) portion of GP1 (7, 8, 12 – 14). Host factors are then proposed to trigger the fusion reaction, possibly by interaction with the remaining fragment of GP1. Recent reports have demonstrated that the endosomal cholesterol transporter Niemann Pick C1 (NPC-1) is critical for EBOV entry, and other unidentified factors may also be required (15, 16). The GP2 subunit contains two heptad repeat regions in the ectodomain (N- and C-terminal, NHR and CHR, respectively) that fold into a stable six-helix bundle. Therefore, the postulated EBOV fusion mechanism is similar to that of HIV-1 gp41 and other members of the structurally defined ‘class I’ family of envelope glycoproteins (3 – 6, 9 – 11). In this model, the N-terminal portion of GP2, which contains a fusion loop, embeds in the host cell membrane following receptor binding to cleaved GP1. This conformational change in GP2 gives rise to a transient intermediate known as the ‘prehairpin’ or ‘extended’ intermediate in which the NHR and CHR are exposed to the extraviral environment. Next, folding of the GP2 six-helix bundle provides the driving force for membrane fusion by pulling the virus and host cell membranes into proximity. The events leading to MARV membrane fusion are presumably similar, since sequences of GP1 and GP2 are highly conserved among these two viruses (17, 18). However, few biochemical studies on the MARV glycoproteins have been reported to date.

The envelope glycoproteins of many viruses that enter the cell via the endosome contain structural

1 elements that drastically affect stability of the pre-fusion conformation (the spike) or the post-fusion
2 conformation in a pH-dependent manner (4 – 6, 19 – 26). In these cases, protonation of one or more
3 side chains drives conformational preferences toward active fusogenic states at low pH (21 – 24). This
4 feature provides a general mechanism for controlling membrane fusion such that it is triggered only
5 when the virus is present in an appropriately matured endosome. For example, low pH-induced
6 conformational changes in the envelope glycoprotein of influenza A virus (HA) results in the exposure
7 of the fusion loop and ultimately its insertion into the host membrane (19, 20). However, the precise
8 residues that are responsible for this transformation vary among strains (27). In the alphavirus Semliki
9 Forest Virus (SFV), the prefusion spike consists of two glycoproteins, E1 and E2, which form a fusion-
10 inactive heterodimer (22 – 24). Protonation of conserved histidine residues in both subunits destabilize
11 the E1-E2 homodimer and promote formation of an E1 trimer, the active fusogenic form of the envelope
12 glycoprotein. In EBOV entry, acidic pH is required to activate CatL and CatB, which have optimal
13 catalytic activity at pH ~5 and whose proteolysis of GP1 is an essential step for infection (12, 13). We
14 recently demonstrated that the folding stability of designed proteins modeled after the six-helix bundle
15 of EBOV GP2 is dependent on pH, with higher stability at lower pH, suggesting that pH alters
16 conformational preferences of the NHR and CHR regions (28). It has been recently reported that
17 peptides corresponding to the fusion loop of EBOV GP2 undergo pH-dependent structural changes that
18 result in increase fusogenic activity at low pH (29). Furthermore, the proteolytically primed form of the
19 GP1/GP2 spike assembly can be activated to bind lipids by treatment with acidic pH or mild reductants
20 (30). Together, these findings suggest a model for EBOV membrane fusion in which the acidification
21 of endosomal compartments triggers the fusogenic machinery of the viral envelope spike.

22 Here we describe the expression, purification, and initial biophysical characterization of the GP2
23 ectodomain from MARV. We found that the MARV GP2 ectodomain forms an α -helical trimer,
24 suggesting a membrane fusion mechanism similar to that of EBOV. Furthermore, we found the stability
25 of the MARV α -helical bundle to be pH-sensitive, with much higher stability under acidic conditions.

1 We performed site-directed mutagenesis to identify residues that are responsible for this behavior.
2
3 Variants containing mutations to several acidic residues in the NHR core trimer and on the external
4
5 CHR α -helices were characterized and found to have altered pH-dependent stability. These results
6
7 suggest that membrane fusion in MARV may also be controlled by pH-dependent stability of the post-
8
9 fusion conformation.
10

11 **MATERIALS AND METHODS**

12
13 *Cloning, Expression, Purification, and Refolding of MARV GP2 Ectodomain.* A synthetic DNA
14
15 fragment encoding 'MarVGP2-C' (see Results) with an N-terminal hexahistidine tag was obtained from
16
17 a commercial supplier (Genewiz, South Plainfield, NJ). This gene was cloned into pET28a (Novagen,
18
19 Madison, WI) with NdeI and XhoI restriction sites to produce the expression plasmid pJH4. Site-
20
21 directed mutagenesis was performed introduce a C557S mutation to yield the expression plasmid pJH5
22
23 (encoding 'MarVGP2-S'). Expression, purification, and refolding of MarVGP2-C and MarVGP2-S
24
25 were similar. *E. coli* BL21 (Invitrogen, Carlsbad, CA) cells harboring pJH4 or pJH5 were grown in LB
26
27 broth at 37 °C to OD₆₀₀ ~0.6, and protein expression induced by addition of 1 mM isopropyl β -D-1
28
29 thiogalactopyranoside (IPTG). The culture was incubated at 37 °C an additional 14-16 hrs. Cells were
30
31 harvested by centrifugation, lysed by stirring in 6 M guanidine HCl (GdnHCl) for 3 hrs at room
32
33 temperature. The cell debris was pelleted by ultracentrifugation and the supernatant was applied
34
35 directly to Ni-NTA resin (Qiagen, Valencia, CA). The resin was washed with 10 column volumes of
36
37 phosphate-buffered saline (PBS) containing 6 M GdnHCl and 50 mM imidazole, then the MarVGP2-C
38
39 or MarVGP2-S protein eluted with PBS containing 6 M GdnHCl and 250 mM imidazole. The eluted
40
41 protein was concentrated, and then further purified by reverse-phase HPLC on a Vydac (Hesperia, CA)
42
43 C18 column (10 μ M, 250 x 21.2 mm) with water/acetonitrile/trifluoroacetic acid mobile phases.
44
45 Fractions containing pure protein were pooled, lyophilized, and redissolved in 6 M GdnHCl. The
46
47 proteins were refolded by step-wise dialysis first into 100 mM glycine HCl pH 3.5, then into 10 mM
48
49 sodium acetate pH 5.3. Protein concentrations were kept below 0.5 mg/mL during the refolding
50
51
52
53
54
55
56
57
58
59
60

1 process. The precipitated material was removed by centrifugation and the refolded protein used
2 immediately for analysis or flash frozen and stored at -80°C .
3

4
5 *Circular Dichroism (CD) Spectroscopy.* Measurements were performed on a Jasco J-815 spectrometer
6 with a 1 cm quartz cuvette. Protein concentrations ranged from 1 – 4 μM as determined by absorbance
7 at 280 nm. Circular dichroism wavelength scans were obtained with an 1 nm step size and a 2 sec
8 averaging time. The signal was converted to mean molar ellipticity (θ) using the equation $\theta = 100 \varepsilon / (n$
9 $l [P]_{\text{tot}})$, where ε is the raw CD signal in degrees, n is the number of amide chromophores, l is the
10 pathlength, and $[P]_{\text{tot}}$ is the protein concentration (31).
11
12
13
14
15
16
17
18

19
20 Chemical and thermal denaturation was monitored at 222 nm ($\theta_{222\text{nm}}$). For chemical denaturation,
21 protein samples were diluted into the appropriate analysis buffer containing varying amounts of
22 GdnHCl, the solution allowed to equilibrate for 1 min, and then $\theta_{222\text{nm}}$ determined. The data were
23 plotted as a function of [GdnHCl], corrected for baseline in folded and unfolded states, then converted
24 to fraction unfolded (F_{unf}) using the equation $[\theta_{222\text{nm}} - \theta_{\text{U}}] / [[\theta_{\text{F}} - \theta_{\text{U}}]$, where θ_{F} and θ_{U} are the CD
25 signals for the folded and unfolded states, respectively. The ΔG_{unf} at each [GdnHCl] concentration was
26 calculated using a monomer-trimer model ($3 M_{\text{U}} \leftrightarrow T_{\text{F}}$, where M_{U} is the unfolded monomer and T_{F} is
27 the folded trimer): $\Delta G_{\text{unf}} = RT \ln \{ 3 F_{\text{unf}}^3 [P]_{\text{tot}}^2 / (1 - F_{\text{unf}}) \}$ where R is the gas constant and T is the
28 absolute temperature (32). The unfolding energy in water ($\Delta G_{\text{unf, H}_2\text{O}}$) was estimated by linear
29 extrapolation to [GdnHCl] = 0 using points in the transition region (33). Thermal denaturation data
30 were obtained with a 3 – 5 $^{\circ}\text{C}$ step size and 2 min equilibration at each temperature. The $\theta_{222\text{nm}}$ was
31 plotted as a function of temperature, corrected for baseline, and converted to F_{unf} . The data were fit to a
32 standard four-parameter logistic equation and the melting temperature, T_{m} , obtained from the inflection
33 point of the curve.
34
35
36
37
38
39
40
41
42
43
44
45
46
47
48
49
50
51
52

53 *Equilibrium Analytical Ultracentrifugation (AU).* Analysis was performed on a Beckman XL-1
54 analytical ultracentrifuge with a Ti60 rotor. Samples of MarVGP2-S were loaded into 1.2 cm cells at a
55 protein concentration of 20 μM , and storage buffer that did not contain protein was used in the reference
56
57
58
59
60

1 cell. Equilibrium sedimentation experiments were carried out at rotor speeds of 12 and 19 kRPM. At
2 each rotor speed, samples were allowed to equilibrate for 24 hrs and the radial spectra collected at 230
3 nm. Comparison of overlaid spectra indicated that there was no mass depletion. The data from both
4 nm. Comparison of overlaid spectra indicated that there was no mass depletion. The data from both
5 rotor speeds were fit globally to a single ideal species model using the program Heteroanalysis
6 (Biotechnology/Bioservices Center, University of Connecticut, Storrs, CT). Non-linear regression was
7 performed in accordance with the expression $c_r = c_o \exp [M (1 - \nu\rho) \omega^2 (r^2 - r_o^2) / 2RT] + \text{base}$, where
8 c_r is the concentration (in absorbance units) at radial position r , c_o is the concentration at an arbitrary
9 reference position r_o near the meniscus, ν is the partial specific volume, ρ is the solvent density, ω is the
10 rotor speed, R is the gas constant, T is the absolute temperature, and base is a baseline absorbance
11 correction to account for non-sedimenting species (34). Molecular weight estimates were obtained from
12 the parameter M . Fits were judged to be adequate if there was no systematic deviation of residuals. A
13 partial specific volume of 0.7337 mL/g was calculated for MarVGP2-S based on amino acid
14 composition, and a solvent density of 1.00182 g/mol was estimated using the program Sednterp
15 (University of New Hampshire).

16
17
18
19
20
21
22
23
24
25
26
27
28
29
30
31
32
33
34 *Structural Modeling and Site-Directed Mutagenesis.* A structural homology model of the MARV GP2
35 ectodomain was generated using the SWISS-MODEL server (<http://swissmodel.expasy.org/>) with the
36 alignment shown in Figure 1A and PDB ID 2EBO as a template (11). This structural model was used to
37 identify positions for analysis by site-directed mutagenesis. Mutant MarVGP2-C or MarVGP2-S clones
38 were prepared using the following protocol. Briefly, pJH4 or pJH5 DNA served as the template for
39 oligonucleotide-based plasmid replication using the primers containing the desired substitutions.
40 Following DNA synthesis, the template DNA was destroyed by digestion with DpnI for 3 hrs at 37 °C,
41 and *E. coli* XL1-Blue (Stratagene, LaJolla, CA) transformed with the resulting mixture. Clones were
42 screened by sequence analysis and those that contained the desired mutations were used for protein
43 production. Preparation of mutant proteins was similar to the wild-type MarVGP2-C and MarVGP2-S
44 (described above) and generally with comparable yields.

RESULTS

Predicted Six-Helix Bundle of the Marburg Virus GP2 Ectodomain. To define the MARV GP2 six-helix bundle, we compared its ectodomain sequence to that of EBOV (*Zaire* strain) GP2 and the structurally related avian sarcoma/leukosis virus (ASLV) Env ectodomains (Figure 1A) (9 – 11, 35, 36). The crystal structures for two variants of the EBOV GP2 ectodomain in the post-fusion state were described previously by Wiley and coworkers (PDB ID 1EBO) (10), and Kim and coworkers (PDB ID 2EBO) (Figure 1B) (11). The EBOV GP2 ectodomain adopts a six-helix bundle with a long, central trimeric coiled-coil core consisting of the NHR segment and three shorter CHR α -helices arranged in an antiparallel configuration about the periphery of the NHR core trimer. An intervening loop region contains a short helix-turn-helix segment that is stabilized by an intramolecular disulfide bond between C601 and C608. The Wiley EBOV GP2 structure contained a trimeric GCN4 segment N-terminal to the NHR to promote solubility and expression (9, 10). Based on the alignment with EBOV GP2 and analysis of these structures, we predicted that a fragment consisting of residues 553-633 of MARV GP2 would adopt a stable six-helix bundle with residues 553-596 forming the NHR core trimer, residues 597-615 forming the loop, and residues 616-633 forming CHR. (Note the amino acid numbering for EBOV GP2 and MARV GP2 differs by one; the numbering for both proteins is shown in Figure 1A). This fragment encompasses the majority of the ectodomain but lacks the fusion loop and the membrane-proximal external region.

Previous work with EBOV GP2 and ASLV Env established disulfide bond connectivity of the three cysteines located at positions 601, 608, and 609 (positions 602, 609, and 610 in MARV GP2) (9 – 11, 35, 36). The residues C601 and C608 in EBOV GP2 form the intramolecular linkage that stabilizes the helix-turn-helix region of the loop between the NHR and CHR, and C609 participates in an intermolecular bridge that tethers GP2 to the surface subunit (GP1) (8). However, both C608 and C609 can both form disulfide bonds with C601 in the isolated EBOV GP2 ectodomain (9 – 11). Therefore, we incorporated a C610S mutation (this position is predicted to participate in the disulfide bond with GP1)

1
2
3
4
5
6
7
8
9
10
11
12
13
14
15
16
17
18
19
20
21
22
23
24
25
26
27
28
29
30
31
32
33
34
35
36
37
38
39
40
41
42
43
44
45
46
47
48
49
50
51
52
53
54
55
56
57
58
59
60

in our MARV GP2 design to prevent heterogeneous disulfide bond formation. The residue C556 is predicted to lie in the α -helical NHR region in the EBOV GP2 post-fusion conformation (10), but this residue participates in a disulfide bridge with C511 to stabilize an antiparallel β -sheet in the pre-fusion conformation (8). The segment between C511 and C556 (EBOV GP2 numbering) is well-conserved among filoviruses and is thought to correspond to the fusion loop (8). The residue C556 was replaced by aspartic acid in the Wiley EBOV GP2 construct and by alanine in the Kim EBOV GP2 construct (10, 11). We prepared two constructs of the MARV GP2 ectodomain: one in which the analogous wild-type C557 side chain was preserved (MarVGP2-C), and a second containing a C557S mutation (MarVGP2-S).

A ‘stutter’ in the periodicity of the NHR heptad repeat pattern was observed in the EBOV GP2 post-fusion conformation (9 – 11). The residue T565 points toward the core of the NHR trimer but occupies a position that, along with the surrounding core NHR residues, results in an unusual 3-4-4-3 hydrophobic repeat (the canonical heptad repeat contains 3-4-3-4 periodicity). This stutter causes a slight distortion of the EBOV NHR α -helix; the alignment in Figure 1A indicates that such a stutter also exists in MARV GP2 (T566) and is included in both MarVGP2-C and MarVGP2-S constructs.

Purification and Characterization of MarVGP2-C and MarVGP2-S. MarVGP2-C and MarVGP2-S proteins were isolated from *E. coli* and refolded by step-wise dialysis first into 100 mM glycine HCl pH 3.5, then into 10 mM sodium acetate buffer (pH 5.3). A portion of protein in each case precipitated during the refolding process; this aggregation could be controlled to some extent by maintaining low protein concentrations (< 0.5 mg/mL). Despite this aggregation, we recovered a reasonable yield of soluble, refolded material through this procedure (~0.1 mg/L of culture). The final refolding buffer did not contain reducing agent in order to allow disulfide bond formation between C602 and C609 (which stabilizes the helix-turn-helix segment). SDS-PAGE analysis under reducing and non-reducing conditions indicated a significant proportion of MarVGP2-C existed as disulfide-bonded oligomers, likely via crosslinks between the unpaired C557 residue on individual chains (see Supporting

Information). In contrast, such crosslinked species were not abundantly observed in MarVGP2-S.

Circular dichroism indicates that both MarVGP2-C and MarVGP2-S are α -helical with double minima at 208 nm and 222 nm in 10 mM sodium acetate, pH 5.3 (Figure 2A). Analytical ultracentrifugation studies under similar conditions at 20 μ M indicate that MarVGP2-S sediments as a single ideal species with a molecular weight of $34,250 \pm 280$ Da (Figure 2B), consistent with a stable trimer (expected trimer molecular weight 33,260 Da). We therefore conclude that MarVGP2-S forms a six-helix bundle, similar to the corresponding regions of EBOV GP2 post-fusion conformation (9 – 11). To estimate the folding stability of MarVGP2-S, we performed chemical denaturation with GdnHCl (Figure 2C). This analysis yielded a $\Delta G_{\text{unf, H}_2\text{O}}$ of 33.4 ± 2.5 kcal/mol when fit to a monomer-trimer model at pH 5.3 (32). To determine whether disulfide bonding between the C602 and C609 contributed to this stability, we performed the GdnHCl denaturation in the presence of the reducing agent tris(hydroxypropyl)phosphine (THP, 2 mM) and found that the protein was markedly destabilized under reducing conditions. The denaturant midpoint, C_m , was 4.7 ± 0.2 M GdnHCl without THP, and 1.4 ± 0.1 with THP. This result indicates that the MARV GP2 C602-609 disulfide bond was oxidized during the refolding protocol and is consistent with observations that the EBOV GP2 ectodomain is stabilized by disulfide bridges between the corresponding C601 and C608 residues (11). In EBOV GP2, the established disulfide bond connectivity of C601-C608 was determined by stability studies with a C609A mutant (which would form an obligate C601-C608 disulfide) and a C608A mutant (obligate C601-C609 disulfide) (11). The C601-C608 disulfide variant displayed enhanced stability relative to the C601-C609 disulfide variant. We did not examine a C602-C610 disulfide variant of MarVGP2-S; however, the highly stable nature of the MarVGP2-S α -helical structure suggests this disulfide bonding pattern is also relevant in MARV GP2.

pH-Dependent Stability. We examined the CD spectra of MarVGP2-S and MarVGP2-C under various buffering conditions and found that the ratio of peaks at 208 nm and 222 nm varied with pH for both proteins (wavelength scans at pH 5.3 and pH 7.0 are shown in Figure 2A). Strong 222 nm signals were

1 observed at pH 5.3 and pH 7.0, indicating significant α -helical character under both of these conditions.
2
3 However, the relative intensities of the 208 nm and 222 nm peaks varied with pH, suggesting
4
5 differences in quaternary packing of α -helical segments (37).
6

7
8 To further explore pH-dependent structural effects, we performed thermal denaturation of
9
10 MarVGP2-S and MarVGP2-C under buffering conditions ranging from pH 4.0 to pH 8.0 using the 222
11
12 nm CD signal to monitor folding (Figure 3 and Table 1). We found that the melting temperature (T_m),
13
14 which provides an estimate of overall folding stability, was sensitive to pH in this range. In 10 mM
15
16 sodium acetate, MarVGP2-S could not be completely unfolded at pH 4.0 and 4.7 (T_m s estimated to be
17
18 ~ 92 and ~ 88 °C, respectively, based on partial unfolding curves), consistent with a highly stable α -
19
20 helical bundle. However, at pH 5.3 full denaturation was observed with a T_m of 75.3 ± 2.1 °C,
21
22 indicating that the unfolding stability is much lower at this pH than at pH 4.0 and 4.7. At pH 6.1 (10
23
24 mM NaOAc buffer) and pH 7.0 (20 mM NaH_2PO_4 buffer), the T_m values were significantly lower (58.8
25
26 ± 1.1 °C and 51.8 ± 0.4 °C, respectively). Similar trends were observed for MarVGP2-C, with T_m
27
28 values ranging from 89.0 ± 0.2 °C at pH 4.0 to ~ 38 °C at pH 8.0 (Figure 3B and Table 1). Figure 3C
29
30 shows T_m as a function of pH for both MarVGP2-S and MarVGP2-C. Overall, the ectodomain
31
32 structural stability is significantly higher at lower pHs, with a ~ 50 °C difference in T_m over the range of
33
34 pH 4.0 to pH 8.0. The pH-dependent stability of MarVGP2-S was confirmed by GdnHCl denaturation
35
36 (Figure 2C); the C_m was significantly higher at pH 5.3 ($C_m = 4.7 \pm 0.2$ M GdnHCl) than at pH 7.0 ($C_m =$
37
38 2.4 ± 0.1 M GdnHCl).
39
40
41
42
43
44
45

46
47 In the GP2 ectodomains structures from EBOV, a conserved central asparagine (N586) in the NHR
48
49 points toward the center of the core and binds monovalent anions (10, 11). This anion-binding pocket
50
51 was also observed in the ectodomain of murine moloney leukemia virus (MoMLV), which is
52
53 structurally similar to EBOV GP2 despite being from a phylogenetically unrelated virus (38). The
54
55 sequence alignment suggests a similar pocket exists in MARV GP2 (N587). In EBOV GP2, the
56
57 presence and nature of the monovalent ion were reported to have moderate effects on thermal stability
58
59
60

1 (the reported T_m s were 84 °C in the presence of 5 mM NaCl or NaBr, 79 °C in 5 mM NaF, and 77 °C
2 without salt) (11). Although the data in Figure 3 and Table 1 were obtained in buffer that did not
3 contain salt, and protein samples were exhaustively dialyzed during the refolding process, we cannot
4 rule out the possibility that trace monovalent anions affected the T_m determinations under various
5 buffering conditions. However, the observed T_m values in various buffering conditions spanned a range
6 of ~50 °C, a much larger range than previously observed with salt effects in EBOV GP2 (range of ~8
7 °C) (11). At both pH 5.3 and pH 7.0, we observed an increase in T_m for MarVGP-C upon addition of
8 500 mM NaCl to the solution (ΔT_m of 5.8 °C at pH 5.3 and 7.7 °C at pH 7.0, Figure 3C and Table 1).
9 However, the stabilization was relatively minor in comparison to the change in stability among the
10 various pH conditions. Furthermore, the T_m at pH 5.3 in the presence of 500 mM NaCl was 18.9 °C
11 higher than that at pH 7.0 with an equivalent amount of salt (78.2 ± 3.0 °C vs. 59.3 ± 1.0 °C).
12 Therefore, we conclude that the salt effects on stability are relatively minor in comparison to the effects
13 of pH.
14
15
16
17
18
19
20
21
22
23
24
25
26
27
28
29
30

31 These results suggest that stability of the MARV GP2 six-helix bundle is sensitive to pH, possibly by
32 protonation of side chain groups. The stabilization of the structure in high salt concentrations may also
33 indicate that charge screening increases stability of the six-helix bundle, further implicating the
34 interaction between ionic groups controls the pH-dependent stability. The pH range of the transition
35 from highly stable (pH 4) to moderately stable (pH 7) occurs in a range that is consistent with pH-
36 dependent stability mediated by acidic residues (Glu and Asp) or histidine residues in the influenza,
37 SFV, and VSV glycoproteins (19 – 26). Similar phenomena were observed in designed protein mimics
38 of the EBOV GP2 α -helical bundle; in this case, the pH-dependent stability was in part due to acidic
39 residues that, when deprotonated, are predicted to disfavor the α -helical bundle formation (28).
40 Mutational studies on the disulfide-containing loop of ASLV Env suggest that this region may play a
41 role in pH-dependent conformational changes for that system (36). Furthermore, the recently reported
42 structure of GP2 from an arenavirus suggest that many intrachain salt bridges stabilize the post-fusion
43
44
45
46
47
48
49
50
51
52
53
54
55
56
57
58
59
60

1 conformation (39).

2
3 *Structural Homology Model and Mutagenesis.* We generated a structural homology model of the
4
5 MARV GP2 ectodomain based on the structure and alignment of the EBOV ectodomain in an attempt to
6
7 determine which residues might be responsible for the pH-dependent stability (Figure 4). The MARV
8
9 GP2 ectodomain contains six total glutamic acid residues, five aspartic acid residues, and a single
10
11 histidine residue (these ionizable side chains are shown in spacefill in Figure 4A). We identified three
12
13 putative side chain-side chain interactions that could potentially contribute to pH-dependent behavior
14
15 (Figures 4B-4D). The residue E580 in MARV corresponds to a heptad repeat core residue L579 in HR1
16
17 of EBOV; the MARV GP2 structural homology model predicts the side chain of this glutamic acid
18
19 residue is oriented toward the core of the trimer (Figure 4B) (10, 11). We hypothesized that this residue
20
21 may be responsible for the pH-dependent stability since, if deprotonated, juxtaposition of E580 anionic
22
23 side chains from opposing monomers to form the central NHR coiled-coil would be unfavorable.
24
25 Similar interactions between acidic residues are observed at the low pH-dependent trimer interface of
26
27 VSV G (26). Variants of the homodimeric coiled-coil GCN4 containing an aspartic acid residue at a
28
29 core *a* position exhibit similar pH-dependent effects (40). At the surface of the model, the side chain of
30
31 E579 on the NHR (E578 in EBOV) is predicted to be near E614 in the loop region (H613 in EBOV)
32
33 (Figure 4C). Contacts between acidic side chains are also observed in the low pH coiled-coils of VSV
34
35 G and influenza HA (20, 26) Furthermore, E622 (D621 or N621 in EBOV, depending on strain) and
36
37 D625 (D624 in EBOV) on the short CHR segment have the capacity to form $i \rightarrow i+3$ intrahelical
38
39 interactions (Figure 4D). We previously reported that similar side chain-side chain anionic residues
40
41 accounted for the pH-dependent stability of the EBOV GP2 six-helix bundle (28). While surface ionic
42
43 interactions in coiled-coils generally have modest effects, it has been shown in several systems that
44
45 additive effects of multiple interactions can play a large role in coiled-coil interactions (41 – 45).
46
47
48
49
50
51
52
53

54 We generated point mutants of MarVGP2-S and MarVGP2-C at positions 579 and 580, and
55
56 examined their thermal stability to explore the role of these positions in the pH-dependent stability. The
57
58
59
60

1 results from these studies are summarized in Table 2. A variant of MarVGP2-C that contained a E579Q
2 mutation at the position predicted to face inward in the core NHR trimer (MarVGP2-CpEQ) was highly
3 unstable at pH 7.0 ($T_m \sim 23$ °C); and a variant containing a E578Q mutation (MarVGP2-CpQE) did not
4
5 exhibit strong α -helical signal under these conditions (this position is predicted to interact with E614).
6
7 These results indicate that neither the E579Q nor the E580Q mutations alone were sufficient to increase
8
9 the stability at pH 7.0. However, a double mutant containing Glu→Gln mutations at both positions
10
11 (MarVGP2-CpQQ) had an unusual thermal denaturation profile with at least two transition phases at pH
12
13 7.0 (Figure 5). Fitting to a multiparameter logistic equation provided two transition temperatures (a
14
15 minor transition, T_1 , and a major transition, T_2) of 27.6 ± 0.5 °C and 74.0 ± 0.2 °C respectively. The
16
17 structural basis of this biphasic thermal unfolding is not clear; in the cases of OmpC and tropomyosin,
18
19 similar behavior has been interpreted to indicate non-cooperative unfolding with each transition
20
21 corresponding to unfolding of a discrete structural element (46, 47). The first transition in MarVGP2-
22
23 CpQQ corresponds to approximately 30% of the CD signal, which is equal to the contribution of the
24
25 CHR segments to total α -helical content of the EBOV GP2 post-fusion structure (10, 11). It is therefore
26
27 possible that the minor transition corresponds to unfolding of the peripheral CHR segments, and the
28
29 major transition corresponds to unfolding of the NHR core trimer. At pH 4.0, the MarVGP2-CpQQ
30
31 clone underwent a single cooperative transition with T_m of 84.1 ± 0.9 °C. Similar behavior was
32
33 observed with a double mutant (E579Q/E580Q) of MarVGP2-S (MarVGP2-SpQQ), though the
34
35 transition temperatures were somewhat different. These results are consistent with a model in which the
36
37 E579Q and E580Q mutations serve to stabilize the core NHR trimer at pH 7.0, but have little or no
38
39 stabilizing effect on the CHR segments.
40
41
42
43
44
45
46
47
48
49

50 To further examine the role of residues E579 and E580, we prepared two additional mutants of
51
52 MarVGP-S: one with an E579K mutation and another with an E580K mutation (MarVGP2-SpEK and
53
54 MarVGP2-SpKE, respectively). We expected that incorporation of a lysine residue at position 580,
55
56 which should maintain a positive charge across a broad pH range, should be more destabilizing to global
57
58
59
60

1 folding stability than an E579K mutation. Indeed, MarVGP2-SpEK was less stable than both
2
3 MarVGP2-SpKE ($\Delta T_m = 21.5$ °C) and MarVGP2-S ($\Delta T_m = 31.0$ °C) at pH 4.7. However, both mutants
4
5 were also less stable than MarVGP2-S at pH 7.0. Together, these results suggest that pH-dependent
6
7 stability of MARV GP2 six-helix bundle is mediated to some degree by E579 and E580.
8

9
10 A variant of MarVGP2-S containing the two mutations E622Q and D625N on the CHR segment
11
12 (MarVGP2-SppQN) was also examined (Table 2). This variant had similar pH-dependent stability to
13
14 the MarVGP2-S, but was less stable at neutral pH. These results suggest that alteration of these two
15
16 acidic side chains to their neutral analog has little effect on the overall pH-dependent stability. Similar
17
18 surface-exposed side chain-side chain residues were postulated to be important for pH-dependent
19
20 stability of α -helical bundle proteins designed from the EBOV GP2 NHR and CHR segments (28).
21
22 Therefore, we conclude such interactions play less of a role in the pH-dependent stability of
23
24 MarVGP2-S.
25
26
27

28 29 **DISCUSSION**

30
31 *Characterization of the MARV GP2 Six-Helix Bundle.* Here we describe the first characterization of the
32
33 MARV GP2 ectodomain; we find this segment adopts a stable trimeric α -helical bundle, consistent with
34
35 the known structures of the phylogenetically related EBOV GP2 and structurally related MoMLV TM
36
37 ectodomains (9 – 11, 38). Chemical denaturation indicates that the MARV GP2 six-helix bundle has a
38
39 folding stability of 33.5 ± 2.5 kcal/mol, which is comparable to the stability of other six-helix bundles
40
41 involved in viral membrane fusion (48, 49). In the model for membrane fusion involving ‘class I’
42
43 envelope glycoproteins (i.e., those with α -helical ectodomains), folding of a six-helix bundle by the
44
45 NHR and CHR segments provides the energetic driving force to overcome the barriers associated with
46
47 fusing the host and viral membranes (4 – 6). Here we show that the relatively short α -helical bundle
48
49 region of MARV GP2 provides a significant amount of folding energy for this task. We further found
50
51 that the disulfide bond between C602 and C609 is required for the overall folding stability and therefore
52
53 likely critical for function.
54
55
56
57
58
59
60

pH-Dependent Stability: Implications for Membrane Fusion. The folding stability of the MARV GP2 ectodomain six-helix bundle, as estimated by T_m , was greatly dependent on pH, with higher stability at lower pH. We previously reported similar pH-dependent stability of α -helical bundle proteins designed from the EBOV GP2 NHR and CHR segments (28). The sensitivity of the six-helix bundle folding to environmental pH may play a role in the process of membrane fusion. It is thought that the post-fusion α -helical bundle is the lowest energy (ground) state conformation. In the pre-fusion state, the ectodomain is prevented from adopting the α -helical bundle by interactions with a surface subunit (e.g., gp120 in HIV-1 or HA in influenza A virus) (3 – 6, 21, 50). A triggering event releases the constraints on the ectodomain when the viral particle is in a suitable environment for membrane fusion to result in productive viral infection (this model is known as the ‘spring-loaded clamp’ model). The precise molecular events that lead to triggering in HIV-1 gp41 and influenza HA have been established; however the details of the EBOV fusion pathway are still under investigation. Furthermore, little is known about MARV entry – it is likely the molecular events are similar to EBOV given the similarity of their envelope glycoprotein sequences, but biological studies indicate there may be some differences in the entry mechanisms (17, 18). For EBOV, it has recently been shown that NPC1 is critical for entry, and this protein may play a role in deployment of the GP2 fusion machinery (15, 16).

We and others have suggested that an additional trigger may be endosomal pH, which serves to increase the stability of the post-fusion six-helix bundle (28, 36). Furthermore, CatL and CatB have optimal activity at pH ~ 5 and recent studies also suggest that the fusion loop may itself have some fusogenic properties that are enhanced in lower pH environments (29, 30). Together, these results suggest that multiple factors involving endosomal resident proteins (NPC1, CatL, and CatB) and endosomal conditions (low pH) work in concert to release constraints on the GP1/GP2 pre-fusion structure, promote formation of the GP2 post-fusion structure, and activate the fusion loop. However, unlike the pH-sensitive transformations observed in influenza HA and SFV E1/E2, in which protonation of specific residues serves to destabilize the pre-fusion conformation (19 – 24), it appears specific

1 protonation events increase the stability of the post-fusion conformation. The results shown here
2 provide the first evidence that a similar mechanism for pH-dependent stabilization of the post-fusion
3 conformation exists in MARV. Furthermore, mutational analysis suggests the pH-dependent stability is
4 controlled to some degree by the acidic residues E579 and E580; the juxtaposition of these anionic
5 residues near other negatively charged residues at neutral pH is predicted to destabilize the post-fusion
6 conformation based on the homology model. An accurate description of the side chain-side chain
7 interactions that stabilize and destabilize the post-fusion conformation awaits a high-resolution crystal
8 structure of the MARV GP2 ectodomain.
9

10 *Models for Thermodynamic and Kinetic Control of pH-Dependent Conformational Changes.* The
11 dramatic structural rearrangement in the central stalk of influenza HA provides a model to distinguish
12 mechanisms of pH-dependent conformational changes (19 – 21, 50, 51). A 36-residue segment, which
13 contains a heptad repeat pattern and is predicted to form a trimeric coiled-coil, is essentially
14 unstructured and monomeric at neutral pH but adopts a highly stable α -helical bundle at low pH (21).
15 Baker and Agard proposed two models to describe how environmental pH could have such a dramatic
16 consequence on the overall fold (Figure 6) (51). In the ‘thermodynamic control’ model, the pH affects
17 the relative stabilities of the lowest energy conformation – at pH 7, the pre-fusion structure represents
18 the ground state. However, at lower pH, the ‘fusion active’ conformation becomes preferred. A
19 defining feature of this model is that the transition from pre-fusion to fusion active conformations is
20 reversible, as would be the effects of pH on the equilibrium. In the ‘kinetic control’ model, the fusion
21 active conformation is the lowest energy structure but a high kinetic barrier maintains the pre-fusion
22 conformation. Exposure to low pH decreases the kinetic barrier, facilitating transition to the lowest
23 energy (fusion active) conformation. The conformational rearrangements in the kinetic model would be
24 irreversible. Early experiments with HA indicate that exposure to low pH does in fact trigger the pH-
25 dependent conformation on the virus; however, this process is irreversible which has led to the
26 conclusion that HA obeys the kinetic control model (3 – 6, 19 – 21). Furthermore, the fusion active
27
28
29
30
31
32
33
34
35
36
37
38
39
40
41
42
43
44
45
46
47
48
49
50
51
52
53
54
55
56
57
58
59
60

1 conformation is adopted spontaneously by synthetic peptides corresponding to the core 36-residue
2 segment at low pH (21), and the fusogenic subunit of HA (HA2) can be refolded into the post-fusion
3 structure at neutral pH suggesting that it is the lowest energy conformation (52). These observations
4 suggest the post-fusion is the lowest energy conformer across all pH conditions.
5
6
7
8

9
10 Other viral membrane fusion proteins, however, appear to exhibit features that are reminiscent
11 of the thermodynamic control model. For example, the envelope glycoprotein G from vesicular
12 stomatitis virus undergoes a pH-dependent transition that appears to be reversible (25, 26). Structural
13 studies suggest that protonation of His residues that are clustered together in the pre-fusion
14 conformation, and of Asp residues that are clustered together in the post-fusion conformation shift the
15 equilibrium toward the post-fusion conformation (25, 26). The core structural feature of the VSV G low
16 pH structure is a six-helix bundle (similar to the class I membrane fusion proteins) and contains a
17 number of acidic residues in proximity. In EBOV, exposure to low pH and mild reductants can trigger
18 the fusogenic properties of the ectodomain on liposomes (30). However, it is unclear if these in vitro
19 triggers fully recapitulate the in vivo fusion cascade, and it is currently unknown whether such
20 treatments are reversible. We have shown that α -helical bundle proteins corresponding to the
21 ectodomains of EBOV and MARV GP2 have pH-dependent stability (28), but these studies have been
22 performed on the isolated proteins alone and it has not been demonstrated that this behavior is relevant
23 to fusion on a viral surface. Therefore, further experiments on the viral surface are required to establish
24 a model for control of the filovirus GP2 conformational changes associated with membrane fusion.
25
26
27
28
29
30
31
32
33
34
35
36
37
38
39
40
41
42
43
44
45
46
47
48
49
50
51
52
53
54
55
56
57
58
59
60

ACKNOWLEDGEMENTS

We thank Michael Brenowitz for assistance with the analytical ultracentrifugation experiments.

SUPPORTING INFORMATION AVAILABLE

SDS-PAGE analysis of purified MarVGP2-S and MarVGP2-C. This material is available free of charge via the Internet at <http://pubs.acs.org>.

REFERENCES

1. Feldmann, H., and Geisbert, T. W. (2011) Ebola haemorrhagic fever. *The Lancet*, 377, 849 – 862.
2. Kuhn, J. H., Becker, S., Ebihara, H., Geisbert, T. W., Johnson, K. M., Kawaoka, Y., Lipkin, W. I., Negrodo, A. I., Netesov, S. V., Nichol, S. T., Palacios, G., Peters, C. J., Tenorio, A., Volchkov, V. E., and Jahrling, P. B. (2010) Proposal for a revised taxonomy of the family Filoviridae: classification, names of taxa and viruses, and virus abbreviations. *Arch. Virol.*, 155, 2083 – 2103.
3. Lee, J. E., and Saphire, E., O. (2009) Ebolavirus glycoprotein structure and mechanism of entry. *Future Virol.*, 4, 621 – 635.
4. Harrison, S. C. (2008) Viral membrane fusion. *Nat. Struct. Mol. Biol.*, 15, 690 – 698.
5. White, J. M., Delos, S. E., Brecher, M., and Schornberg, K. (2008) Structures and mechanisms of viral membrane fusion proteins: Multiple variations on a common theme. *Crit. Rev. Biochem. Mol. Biol.*, 43, 189 – 219.
6. Eckert, D. M., and Kim, P. S. (2001) Mechanisms of viral membrane fusion and its inhibition. *Annu. Rev. Biochem.*, 70, 777 – 810.
7. Lee, J. E., Fusco, M. L., Hessel, A. J., Oswald, W. B., Burton, D. R., Saphire, E. O. (2008) Structure of the Ebola virus glycoprotein bound to an antibody from a human survivor. *Nature*, 454, 177 – 182.
8. Dias, J. M., Kuehne, A. I., Abelson, D. M., Bale, S., Wong, A. C., Halfmann, P., Muhammad, M. A., Fusco, M. L., Zak, S. E., Kang, E., Kawaoka, Y., Chandran, K., Dye, J. M., and Saphire, E. O. (2011) A shared structural solution for neutralizing ebolaviruses. *Nat. Struct. Mol. Biol.*, 18, 1424 – 1427.
9. Weissenhorn, W., Calder, L. J., Wharton, S. A., Skehel, J. J., and Wiley, D. C. (1998) The central structural feature of the membrane fusion protein subunit from the Ebola virus glycoprotein is a long triple-stranded coiled coil. *Proc. Natl. Acad. Sci. USA*, 95, 6032 – 6036.
10. Weissenhorn, W., Carfi, A., Lee, K. H., Skehel, J. J., and Wiley, D. C. (1998) Crystal structure of

- 1 the Ebola virus membrane fusion subunit, GP2, from the envelope glycoprotein ectodomain. *Mol.*
2
3 *Cell*, 2, 605 – 616.
- 4
5 11. Malashkevich, V. N., Schneider, B. J., McNally, M. L., Milhollen, M. A., Pang, J. X., and Kim PS.
6
7 (1999) Core structure of the envelope glycoprotein GP2 from Ebola virus at 1.9-Å resolution. *Proc.*
8
9 *Natl. Acad. Sci. USA*, 96, 2662 – 2667.
- 10
11 12. Chandran, K., Sullivan, N. J., Felbor, U., Whelan, S. P., and Cunningham, J. M. (2005) Endosomal
12
13 proteolysis of the Ebola virus glycoprotein is necessary for infection. *Science*, 308, 1643 – 1645.
- 14
15 13. Schornberg, K., Matsuyama, S., Kabsch, K., Delos, S., Bouton, A., White, J. (2006) Role of
16
17 endosomal cathepsins in entry mediated by the Ebola virus glycoprotein. *J. Virol.*, 80, 4174 – 4178.
- 18
19 14. Dube, D., Brecher, M. B., Delos, S. E., Rose, S. C., Park, E. W., Schornberg, K. L., Kuhn, J. H., and
20
21 White, J. M. (2009) The primed ebolavirus glycoprotein (19-kilodalton GP1,2): sequence and
22
23 residues critical for host cell binding. *J. Virol.*, 83, 2883 – 2891.
- 24
25 15. Carette, J. E., Raaben, M., Wong, A. C., Herbert, A. S., Obernosterer, G., Mulherkar, N., Kuehne,
26
27 A. I., Kranzusch, P. J., Griffin, A. M., Ruthel, G., Dal Cin, P., Dye, J. M., Whelan, S. P., Chandran,
28
29 K., and Brummelkamp, T. R. (2011) Ebola virus entry requires the cholesterol transporter
30
31 Niemann-Pick C1. *Nature*, 477, 340 – 343.
- 32
33 16. Côté, M., Misasi, J., Ren, T., Bruchez, A., Lee, K., Filone, C. M., Hensley, L., Li, Q., Ory, D.,
34
35 Chandran, K., and Cunningham, J. (2011) Small molecule inhibitors reveal Niemann-Pick C1 is
36
37 essential for Ebola virus infection. *Nature*, 477, 344 – 348.
- 38
39 17. Battacharyya, S., Hope, T. J., and Young, J. A. (2011) Differential requirements for clathrin
40
41 endocytic pathway components in cellular entry by Ebola and Marburg glycoprotein pseudovirions.
42
43 *Virology*, 419, 1 – 9.
- 44
45 18. Matsuno, K., Kishida, N., Usami, K., Igarashi, M., Yoshida, R., Nakayama, E., Shimojima, M.,
46
47 Feldmann, H., Irimura, T., Kawaoka, Y., and Takada, A. (2010) Different potential of C-type
48
49 lectin-mediated entry between Marburg virus strains. *J. Virol.*, 84, 5140 – 5147.
- 50
51
52
53
54
55
56
57
58
59
60

- 1 19. Bullough, P. A., Hughson, F. M., Skehel, J. J., and Wiley, D. C. (1994) Structure of the influenza
2 haemagglutinin at the pH of membrane fusion. *Nature*, *371*, 37 – 43.
- 3
- 4 20. Wilson, I. A., Skehel, J. J., and Wiley, D. C. (1981) Structure of the haemagglutinin membrane
5 glycoprotein of influenza virus at 3Å resolution. *Nature*, *289*, 366 – 373.
- 6
- 7 21. Carr, C. M., and Kim, P. S. (1993) A spring-loaded mechanism for the conformational change of
8 influenza hemagglutinin. *Cell*, *73*, 823 – 832.
- 9
- 10 22. Sánchez-San Martín, C., Liu, C. Y., and Kielian, M. (2009) Dealing with low pH: entry and exit of
11 alphaviruses and flaviviruses. *Trends Microbiol.*, *17*, 514 – 521.
- 12
- 13 23. Fritz, R., Stiasny, K., and Heinz, F. X. (2008) Identification of specific histidines as pH sensors in
14 flavivirus membrane fusion. *J. Cell Biol.*, *183*, 353 – 361.
- 15
- 16 24. Qin, Z. L., Zheng, Y., and Kielian M (2009) Role of conserved histidine residues in the low pH
17 dependence of the Semliki Forest virus fusion protein. *J. Virol.*, *83*, 4670 – 4677.
- 18
- 19 25. Roche, S., Rey, F. A., Gaudin, Y., and Bressanelli, S. (2007) Structure of the prefusion form of the
20 vesicular stomatitis virus glycoprotein G. *Science*, *315*, 843 – 848.
- 21
- 22 26. Roche, S., Bressanelli, S., Rey, F. A., and Gaudin, Y. (2006) Crystal structure of the low-pH form
23 of the vesicular stomatitis virus glycoprotein G. *Science*, *313*, 187 – 191.
- 24
- 25 27. Daniels, R. S., Downie, J. C., Hay, A. J., Knossow, M., Skehel, J. J., Wang, M. L., and Wiley, D. C.
26 (1985) Fusion mutants of the influenza virus hemagglutinin glycoprotein. *Cell*, *40*, 431 – 439.
- 27
- 28 28. Harrison, J. S., Higgins, C. D., Chandran, K., and Lai, J. R. (2011) Designed protein mimics of the
29 Ebola virus glycoprotein GP2 α -helical bundle: Stability and pH effects. *Protein Sci.*, *20*, 1587 –
30 1596.
- 31
- 32 29. Gregory, S. M., Harada, E., Liang, B., Delos, S. E., White, J. M., and Tamm LK. (2011) Structure
33 and function of the complete internal fusion loop from Ebolavirus glycoprotein 2. *Proc. Natl. Acad.*
34 *Sci. USA*, *108*, 11211 – 11216.
- 35
- 36 30. Brecher, M., Schornberg, K. L., Delos, S. E., Fusco, M. L., Sapphire, E. O., and White, J. M. (2012)
- 37
- 38
- 39
- 40
- 41
- 42
- 43
- 44
- 45
- 46
- 47
- 48
- 49
- 50
- 51
- 52
- 53
- 54
- 55
- 56
- 57
- 58
- 59
- 60

1 Cathepsin cleavage potentiates the Ebola virus glycoprotein to undergo a subsequent fusion-relevant
2 conformational change. *J. Virol.*, *86*, 364 – 372.

- 3
4
5 31. Cantor, C. R.; Schimmel, P. R. *Biophysical Chemistry, Part II: Techniques for the study of*
6 *biological structure and function*. 1998, W. H. Freeman and Company: New York, NY. pp426 –
7 428,
8
9
10
11 32. Boice, J. A., Dieckmann, G. R., Degrado, W. F., and Fairman, R. (1996) Thermodynamic analysis
12 of a designed three-stranded coiled coil. *Biochemistry*, *35*, 14480 – 14485.
13
14
15 33. Pace, C. N. (1986) Determination and analysis of urea and guanidine hydrochloride denaturation
16 curves. *Methods Enzymol.*, *131*, 266 – 280.
17
18
19 34. Schuster, T. M.; Laue, T. M., Eds. *Modern analytical ultracentrifugation 1994*, Birkhauser: Boston,
20 MA. pp3 – 15.
21
22
23 35. Gallaher, W. R. (1996) Similar structural models of the transmembrane proteins of Ebola and
24 Avian Sarcoma viruses. *Cell*, *85*, 477 – 478.
25
26
27 36. Delos, S. E., La, B., Gilmartin, A., and White, J. M. (2010) Studies of the "chain reversal regions"
28 of the avian sarcoma/leukosis virus (ASLV) and ebolavirus fusion proteins: analogous residues are
29 important, and a His residue unique to EnvA affects the pH dependence of ASLV entry. *J. Virol.*,
30 *84*, 5687 – 5694.
31
32
33 37. Lau, S. Y., Taneja, A. K., and Hodges, R. S. (1984) Synthesis of a model protein of defined
34 secondary and quaternary structure: Effect of chain length on the stabilization and formation of two-
35 stranded α -helical coiled-coils. *J. Biol. Chem.*, *259*, 13253 – 13261.
36
37
38 38. Fass, D., Harrison, S. C., and Kim, P. S. (1996) Retrovirus envelope domain at 1.7 angstrom
39 resolution. *Nat. Struct. Biol.*, *3*, 465 – 469.
40
41
42 39. Igonet, S., Vaney, M. C., Vonhrein, C., Bricogne, G., Stura, E. A., Hengartner, H., Eschli, B., and
43 Rey, F. A. (2011) X-ray structure of the arenavirus glycoprotein GP2 in its postfusion hairpin
44 conformation. *Proc. Natl. Acad. Sci. USA*, *108*, 19967 – 19972.
45
46
47
48
49
50
51
52
53
54
55
56
57
58
59
60

- 1
2
3
4
5
6
7
8
9
10
11
12
13
14
15
16
17
18
19
20
21
22
23
24
25
26
27
28
29
30
31
32
33
34
35
36
37
38
39
40
41
42
43
44
45
46
47
48
49
50
51
52
53
54
55
56
57
58
59
60
40. Lau, W. L., Degrado, W. F., and Roder, H. (2010) The effects of pKa tuning on the thermodynamics and kinetics of folding: design of a solvent-shielded carboxylate pair at the α -position of a coiled-coil. *Biophys. J.*, *99*, 2299 – 2308.
 41. Kohn, W. D., Cyril, M. K., and Hodges, R. S. (1995) Protein destabilization by electrostatic repulsions in the two-stranded α -helical coiled-coil/leucine zipper. *Protein Sci*, *4*, 237 – 250.
 42. Scholtz, J. M., Qian, H., Robbins, V. H., and Baldwin, R. L. (1993) The energetics of ion-pair and hydrogen-bonding interactions in a helical peptide. *Biochemistry*, *32*, 9668 – 9676.
 43. O’Shea, E. K., Lumb, K. J., and Kim, P. S. (1993) Peptide ‘Velcro’: design of a heterodimeric coiled-coil. *Curr, Biol.*, *3*, 658 – 667.
 44. O’Shea, E. K., Rutkowski, R., and Kim, P. S. (1992) Mechanism of specificity in the Fos-Jun oncoprotein heterodimer. *Cell*, *68*, 699 – 708.
 45. Lumb, K. J., and Kim, P. S. (1995) Measurement of interhelical electrostatic interactions in the GCN4 leucine zipper. *Science*, *268*, 436 – 439.
 46. Keegan, N., Ridley, H., and Lakey, J. H. (2010) Discovery of biphasic thermal unfolding of OmpC with implications for surface loop stability. *Biochemistry*, *49*, 9715 – 9721.
 47. Heller, M. J., Nili, M., Homsher, E., and Tobacman, L. S. (2003) Cardiomyopathic tropomyosin mutations that increase thin filament Ca^{2+} sensitivity and tropomyosin N-domain flexibility. *J. Biol. Chem.*, *278*, 41742 – 41748.
 48. Jelesarov, I., and Lu, M. (2001) Thermodynamics of trimer-of-hairpins formation by the SIV gp41 envelope glycoprotein. *J. Mol. Biol.*, *307*, 637 – 656.
 49. Marti, D. N., Bjelic, S., Lu, M., Bosshard, H. R., and Jelesarov, I. (2004) Fast folding of the HIV-1 and SIV gp41 six-helix bundles. *J. Mol. Biol.*, *336*, 1 – 8.
 50. Carr, C. M., Chaudry, C., and Kim, P. S. (1997) Influenza hemagglutinin is spring-loaded by a metastable native conformation. *Proc. Natl. Acad. Sci. USA*, *94*, 14306 – 14313.
 51. Baker, D., and Agard, D. A. (1994) Influenza hemagglutinin: Kinetic control of protein function.

1 *Structure*, 2, 907 – 910.

2
3 52. Swalley, S. E., Baker, B. M., Calder, L. J., Harrison, S. C., Skehel, J. J., and Wiley, D. C. (2004)

4 Full-length influenza hemagglutinin HA2 refolds into the trimeric low-pH-induced conformation.

5
6
7 *Biochemistry*, 43, 5902-5911.

8
9
10
11
12
13
14
15
16
17
18
19
20
21
22
23
24
25
26
27
28
29
30
31
32
33
34
35
36
37
38
39
40
41
42
43
44
45
46
47
48
49
50
51
52
53
54
55
56
57
58
59
60

TABLES

Table 1 – Stability of MarVGP2-S and MarVGP2-C under Various Buffering Conditions.

Buffering condition	T _m (°C) ^A
<i>MarVGP2-S</i>	
10 mM NaOAc, pH 4.0	~92 ^B
10 mM NaOAc, pH 4.7	~88 ^B
10 mM NaOAc, pH 5.3	75.3 ± 2.1
10 mM NaOAc, pH 5.7	65.1 ± 1.0
10 mM NaOAc, pH 6.1	58.8 ± 1.1
20 mM NaHPO ₄ , pH 7.0	51.8 ± 0.4
<i>MarVGP2-C</i>	
10 mM NaOAc, pH 4.0	89.0 ± 0.2
10 mM NaOAc, pH 4.8	86.9 ± 0.3
10 mM NaOAc, pH 5.3	72.4 ± 1.4
10 mM NaOAc, pH 6.1	47.0 ± 1.5
20 mM NaHPO ₄ , pH 7.0	51.6 ± 1.3
20 mM NaHPO ₄ , pH 8.0	~38 ^C
10 mM NaOAc, pH 5.3 + 500 mM NaCl	78.2 ± 3.0
20 mM NaHPO ₄ , pH 7.0 + 500 mM NaCl	59.3 ± 1.0

^A Errors listed here represent 95% confidence interval from data fitting.

^B Complete unfolding was not observed at 100 °C, an estimate for T_m is provided based on fitting the partial unfolding curve.

^C A broad thermal transition prevented accurate determination of T_m.

Table 2 – Summary of Results from Analysis of MarVGP2-S and MarVGP2-C Mutants

Variant	Mutation(s)	$T_m^{(pH \sim 4.7)} (^{\circ}C)^A$	$T_m^{(pH 7.0)} (^{\circ}C)^A$	$\Delta T_m (^{\circ}C)$
MarVGP2-C (WT)	N/A	86.9 ± 0.3	51.6 ± 1.3	35.3
MarVGP2-CpQE	E579Q	ND	(not stable)	--
MarVGP2-CpEQ	E580Q	ND	$\sim 23^{\circ}C$	--
MarVGP2-CpQQ	E579Q/E580Q	84.1 ± 0.9	$T_1, 27.6 \pm 0.5$ $T_2, 74.0 \pm 0.2$	--
MarVGP2-S (WT)	N/A	~ 88	51.8 ± 0.4	~ 36
MarVGP2-SpQQ	E579Q/E580Q	81.5 ± 3.5	$T_1, 32.2 \pm 3.8$ $T_2, 69.9 \pm 0.6$	--
MarVGP2-SpKE	E579K	76.9 ± 3.2	$\sim 39^B$	~ 38
MarVGP2-SpEK	E580K	54.8 ± 1.1	$\sim 20^B$	~ 35
MarVGP2-SppQN	E622Q/D625N	83.5 ± 0.4	41.6 ± 2.1	41.9

^A Errors listed here represent 95% confidence interval from data fitting.

^B N/A, not applicable; ND, not determined.

^C A broad thermal transition prevented accurate determination of T_m .

FIGURE CAPTIONS

Figure 1. (A) Sequence alignment of GP2 from *Zaire ebolavirus* (EBOV), ASLV, and MARV (residues that differ from EBOV shown colored gray). The amino acid numbering for EBOV GP2 and MARV GP2 differ by one; the EBOV numbering is shown above the sequence alignment and the MARV numbering shown below. The regions corresponding to the NHR, CHR, and helix-turn-helix regions of EBOV GP2 are indicated with cylinders whose colors match the structural elements depicted in panel B. Established disulfide bond connectivities are shown, and glycosylation sites are indicated with an 'o'. The T565 (EBOV numbering) residue that gives rise to the unusual 3-4-4-3 hydrophobic stutter in the NHR is indicated with an 'x', other residues in the NHR that form core positions are denoted *a* and *d*. The C556 (EBOV numbering) residue in NHR is indicated with an asterisk (below). (B) Crystal structures of the EBOV GP2 ectodomain reported by Wiley and coworkers (ref. 10, PDB ID 1EBO), and Kim and coworkers (ref. 11, PDB ID 2EBO). In the Wiley structure, the trimeric GCN4 tag is shown in cyan.

Figure 2. Biophysical characterization of the MARV GP2 ectodomain. (A) CD spectra of MarVGP2-S in 10 mM sodium acetate, pH 5.3 and 10 mM sodium phosphate, pH 7.0 (B) Representative analytical ultracentrifugation at pH 5.3. High-resolution data were obtained at 12 and 19 krpm rotor speeds and fit to a single ideal species model to yield a molecular weight estimate consistent with a trimer (see text). (c) Guanidine HCl denaturation of MarVGP2-S in 10 mM NaOAc pH 5.3 in the absence and presence of the reducing agent THP, and in 20 mM NaH₂PO₄, pH 7.0. The denaturant midpoint (C_m) values are 4.7 ± 0.2 M GdnHCl at pH 5.3, 1.4 ± 0.1 M GdnHCl at pH 5.3 with THP, and 2.4 ± 0.1 M GdnHCl at pH 7.0. Linear extrapolation on the pH 5.3 data yielded $\Delta G_{\text{unf,H}_2\text{O}} = 33.4 \pm 2.5$ kcal/mol (inset).

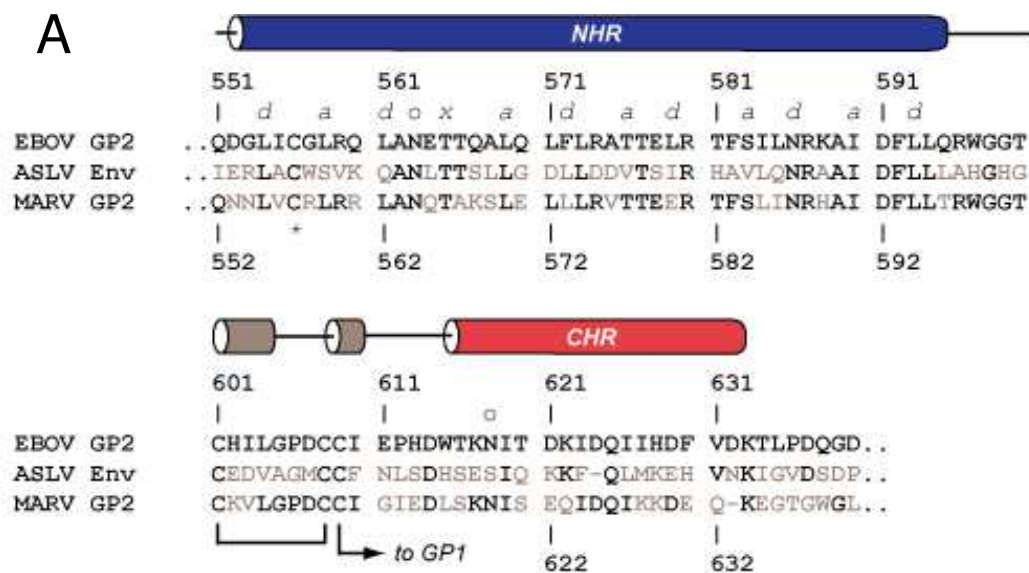
Figure 3. pH-Dependent thermal stability of the MARV GP2 α -helical bundle as monitored by $[\theta]_{222}$. Thermal denaturation curves of MarVGP2-S (A) and MarVGP2-C (B) under various buffering conditions. (C) Plot of T_m vs. pH.

1 **Figure 4.** (A) Structural homology model of MARV GP2 ectodomain based on the crystal structure of
2 EBOV GP2 (ref. 11, PDB ID 2EBO). Glutamic acid (yellow), aspartic acid (green), and histidine
3 (orange) residues are shown in spacefill. (B-C) Predicted interactions that could destabilize the six-
4 helix bundle, shown in spacefill. (B-C) Predicted interactions that could destabilize the six-
5 helix bundle, shown in stick and colored by atom for clarity: (B) E580 interactions in the NHR core
6 trimer; (C) E579-E614 interaction between opposing monomers; (D) E622-D625 $i \rightarrow i+3$ intrahelical
7 interaction.
8
9
10
11
12
13

14 **Figure 5.** Denaturation profiles of MarVGP2-CpQQ and MarVGP2-SpQQ at pH 4.7 and pH 7.0.
15
16

17 **Figure 6.** Thermodynamic control and kinetic control models for pH-dependent conformational
18 rearrangements.
19
20
21
22
23
24
25
26
27
28
29
30
31
32
33
34
35
36
37
38
39
40
41
42
43
44
45
46
47
48
49
50
51
52
53
54
55
56
57
58
59
60

FIGURE 1

**B**PDB ID 1EBO
(Wiley and coworkers)PDB ID 2EBO
(Kim and coworkers)

(Trimeric GCN4)

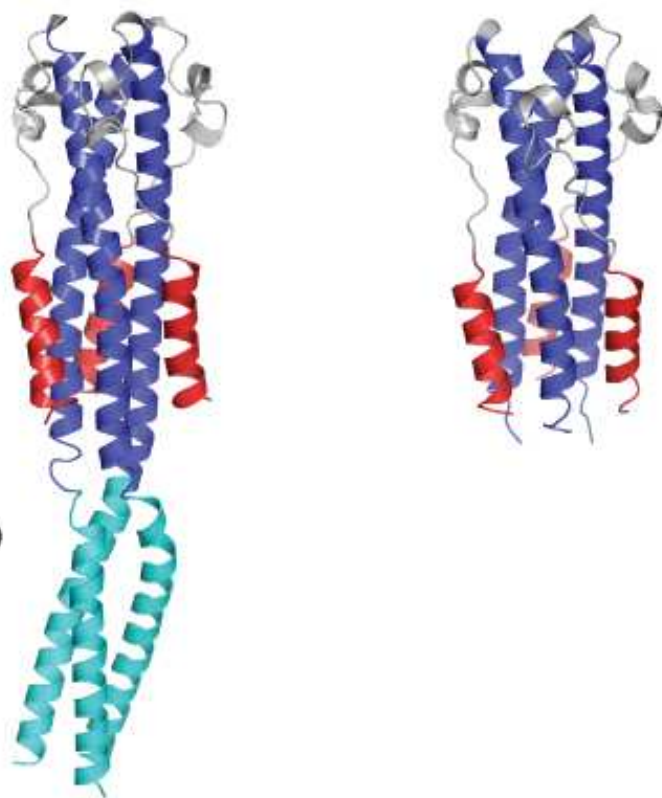


FIGURE 2

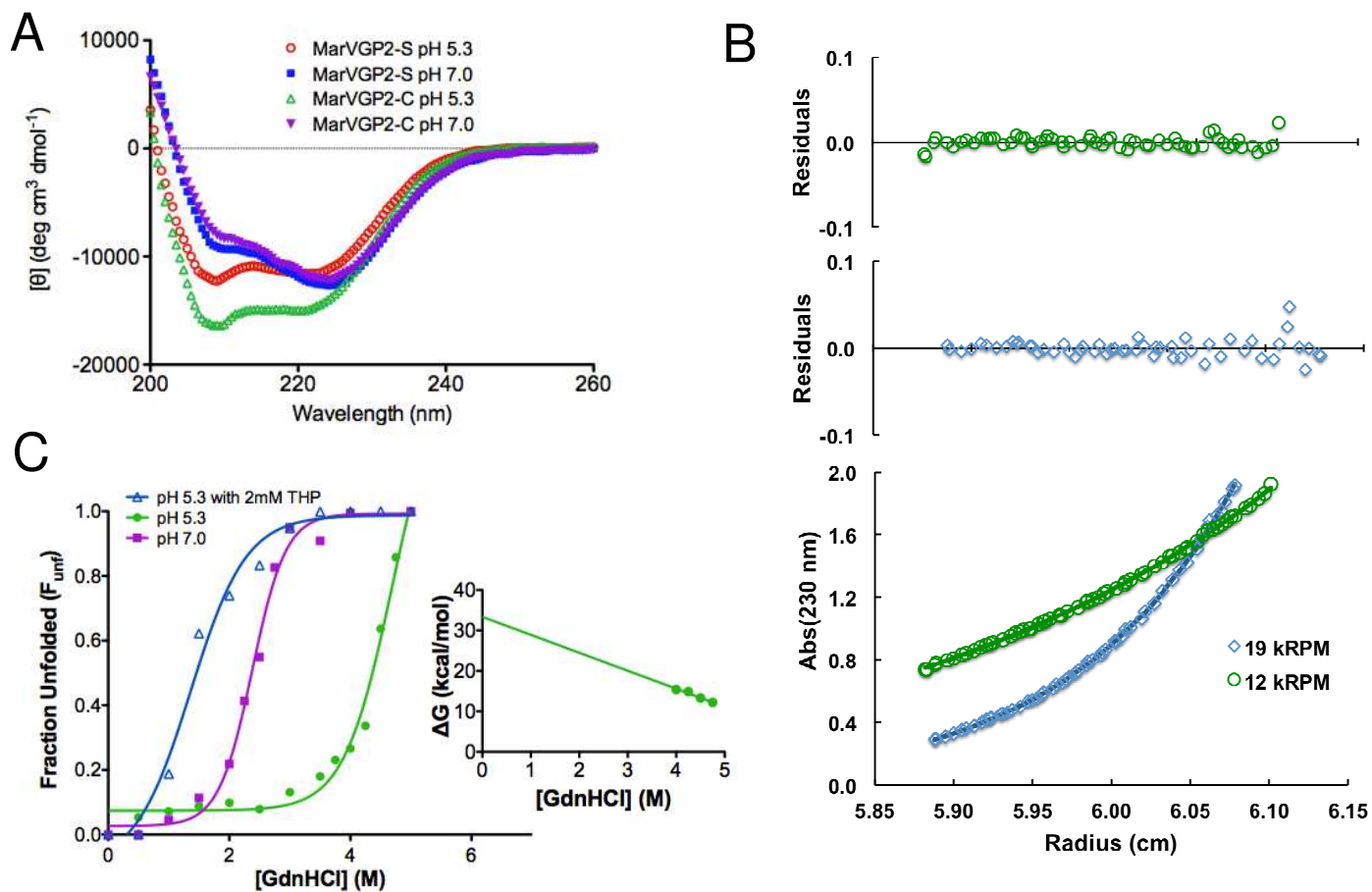


FIGURE 3

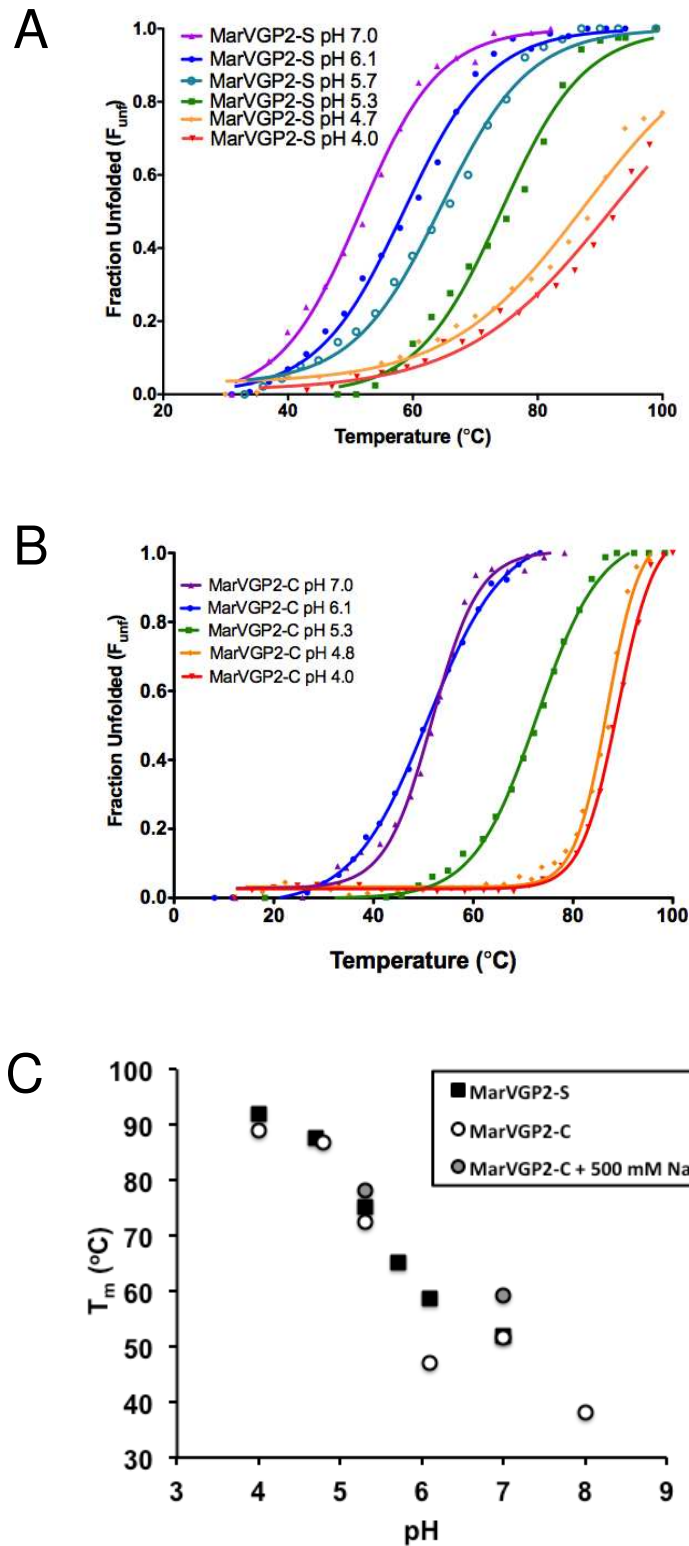


FIGURE 4

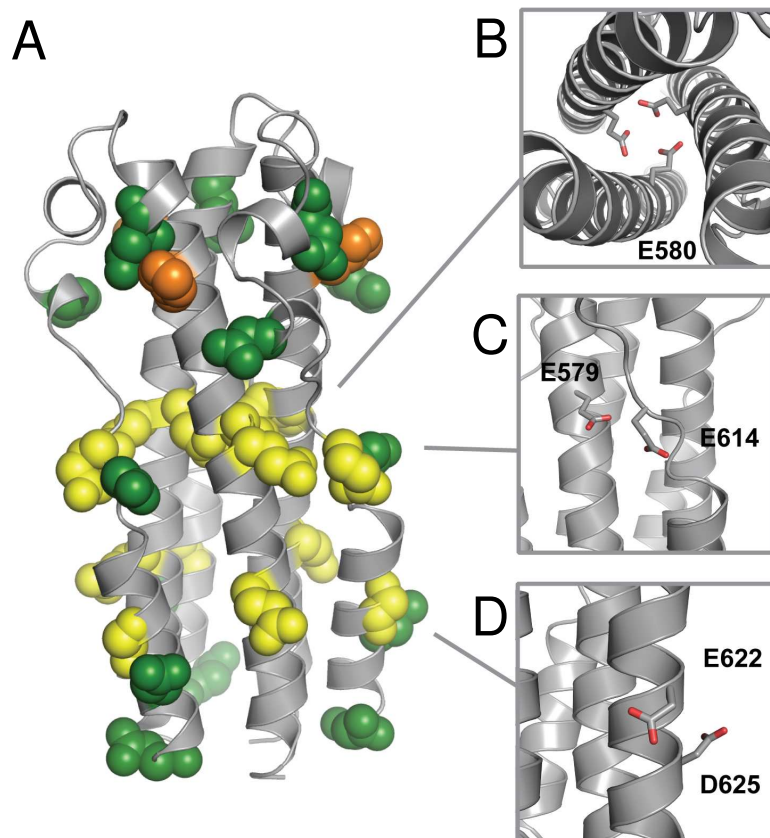


FIGURE 5

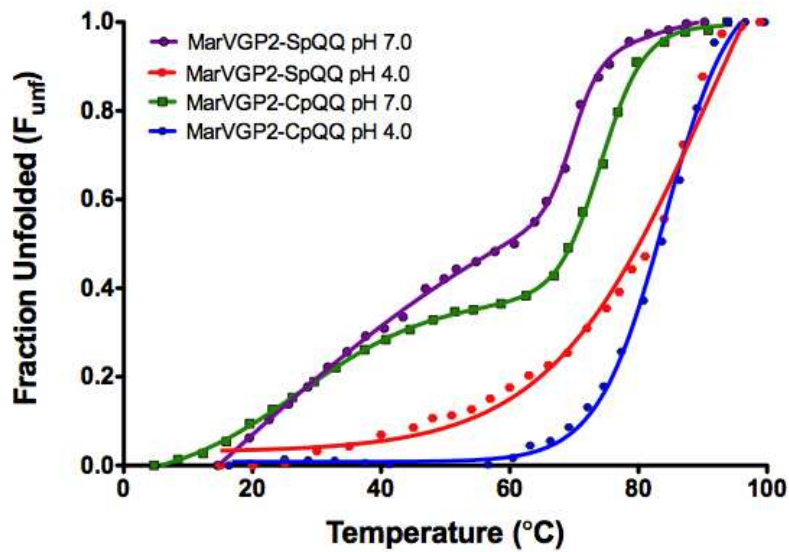
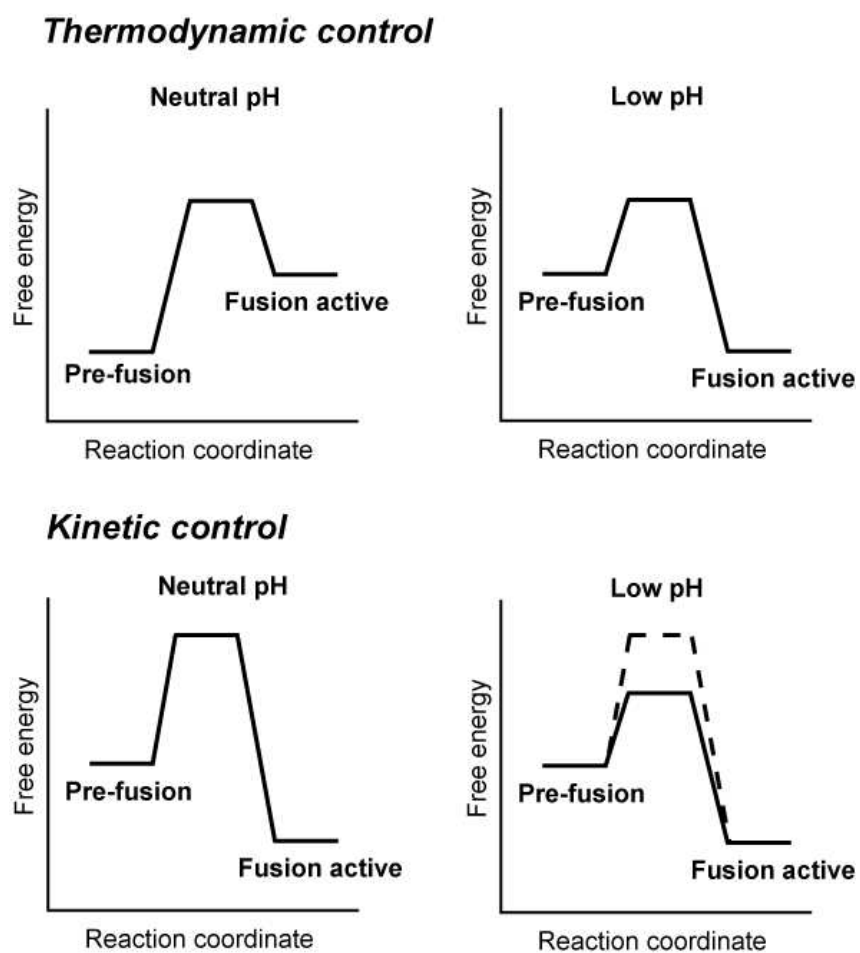


FIGURE 6



1
2
3
4
5
6
7
8
9
10
11
12
13
14
15
16
17
18
19
20
21
22
23
24
25
26
27
28
29
30
31
32
33
34
35
36
37
38
39
40
41
42
43
44
45
46
47
48
49
50
51
52
53
54
55
56
57
58
59
60

FOR TABLE OF CONTENTS USE ONLY

Marburg Virus Glycoprotein GP2: pH-Dependent Stability of the Ectodomain α -Helical Bundle

Joseph S. Harrison, Jayne F. Koellhoffer, Kartik Chandran, and Jonathan R. Lai

